ISSN(PRINT) : 2320 -1967
ISSN(ONLINE) : 2320 -1975
GLOBAL SCIENTIFIC INC.
ChemXpress

ORIGINAL ARTICLE

CHEMXPRESS 9(2), 109-118, (2016)

Study of silane layers grown on steel and characterized using ellipsometry at different wavelengths and incidence angles

P.R.Seré[1,4], J.O.Zerbino[2]*, A.Maltz[3], C.Deya[1,4], C.I.Elsner[1,4], A.R.Di Sarli[1]

[1]CIDEPINT: Centro de Investigación y Desarrollo en Tecnología de Pinturas (CICPBA-CONICET La Plata). Av. 52, entre 121 y 122. (CP. 1900) La Plata, (ARGENTINA)
[2]INIFTA, Instituto de Investigaciones Fisicoquímicas, Teóricas y Aplicadas (CONICET, CICPBA, UNLP). C.C. 16 Suc.4. (CP. 1900) La Plata, (ARGENTINA)
[3]Departamento de Matemática. UNLP, (ARGENTINA)
[4]Facultad de Ingeniería, UNLP, Av. 1 esq. 45. (CP. 1900) La Plata, (ARGENTINA)
E-mail: jzerbino@inifta.unlp.edu.ar
Received : 09th February, 2015 ; Revised : 11th June, 2015 ; Accepted : 20th June, 2015

Abstract : Films of gmercap to propyltri methoxysilane are prepared by hydrolysis, condensation and curing at 80 °C. The optical indices, n, k and the thickness d are calculated using the ellipsometry technique. A programme is developed to fit a wide set of ellipsometric Δ and Ψ data in the visible optical region 400 nm < λ < 600 nm. An increase in the optical absorption *k* is detected for the lower concentration of MPTMS attributed to light absorption from the pores.

Keywords : Mercaptopropyltrimethoxysilane; Ellipsometry; Anticorrosive coating; Optical constants.

INTRODUCTION

Organ functional silanes improve the adhesion between organic polymers and inorganic materials[1]. Silanes compounds are claimed to replace chromium compounds in temporarily anticorrosive protection. Compared to chromate conversion coatings with a thickness greater than 5 μm, the siloxane layers are extraordinarily thin. The barrier effect strongly depends on the nature of the used siloxane coating[2], while the film thickness, on the order of some hundred nanometers depends on the silane type and the concentration as well as on the curing conditions[3-6]. A nearly linear dependence of the film thickness on the concentration of silanes in the aqueous solution was reported[2].

The γmercaptopropyltrimethoxysilane (MPTMS) can be used as adhesion promoter to provide surface protection, and also for the development of integrated circuits in the organic thin film transistors

ORIGINAL ARTICLE

(OTFT) industry, in wear-resistant coatings, solid oxide fuel cells and oxygen sensors[7-9].

The precursor MPTMS has the formula S-R-Si-$(OCH_3)_3$ with two reactive groups: The first one is the -OCH_3 methoxy which hydrolyses resulting –Si-OH silanol capable to form covalent bounds with a) other –Si-OH groups forming the –Si-O-Si- siloxane network and b) with the surface hydroxide of the ferric alloys. The second is the tiol group -SH which can react forming strong covalent bounds with Ag, Au, Pt or Cu[9]

By hydrolysis and condensation, the MPTMS forms mesoporous layers used as "primer" for improving the adhesion of anticorrosive coatings[9]. The conditions for the silane hydrolysis and the curing of the film formed on the metal depend on the metal to protect and the silanes type[4, 10]. Copper and hot deep electrogalvanized steel were protected by films obtained from different MPTMS solutions with good results[11, 12]. The silane film protects the metal against corrosion by barrier effect, inhibiting the arrival of aggressive ions and water to the substrate[13-15]. Therefore, the thickness, uniformity and porosity of the silane film are of vital importance in the degree of protection afforded for the substrate[3, 16].

Ellipsometry is one of the most suitable techniques used to measure the thickness, porosity and uniformity of silane coatings[6, 15]. Several articles have used ellipsometry to estimate the thickness of coats assumed as non absorbing layers, i.e. optical absorption $k \approx 0$[2, 7, 9, 17-20]. However, the presence of pores can produce an increase of k which, in turn, can have a significant effect upon the calculated *n* and *d* values.

In this paper the optical parameters for two or three coating steps are fitted assuming an isotropic and homogeneous film. The global treatment of data (obtained at different wavelengths, λ, and incident angles, ϕ, 65°, 69° or 74°) increases the accuracy of the calculated optical parameters leading to a univocal mathematical solution which becomes independent of the initial parameters used in the fitting.

EXPERIMENTAL

The solution was prepared by mixing 8.0 ml of MPTMS in 92.0 ml of ethanol / water (15 / 1, by volume). The pH of the water / ethanol solution was previously adjusted to 4 with acetic acid. In a final step, the suspension was stirred for 1 hour to obtain a stable hydrolyzed silane solution, which results in a maximum amount of reactive silanol groups interacting with the surface oxide (Procedure I)[11-12]. In order to obtain a 4% silane final concentration (Procedure II) a volume of the above mentioned solution was diluted with the same volume of the ethanol/ water solution, 1:1 dilution degree.

SAE 1010 steel sheets were used as substrate and the samples were polished with diamond paste of 0.25 μm to achieve specular surface. Silane coatings were applied by dipping the steel samples into MPTMS solutions of two concentrations 8% (Procedure I) and 4% (Procedure II) for 100 s, subsequently blow drying with compressed air to remove

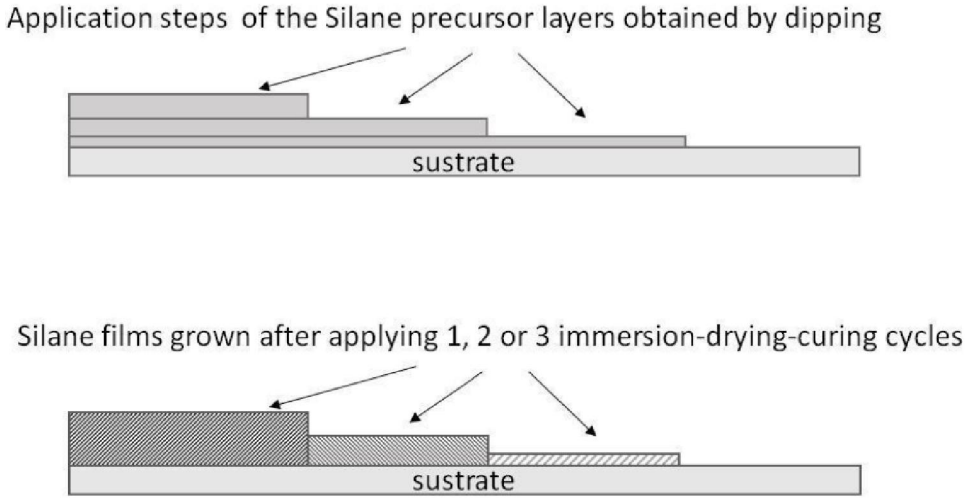

Figure 1 : Sample preparation: a) Application steps of the silanes. b) Silanes film after the curing process.

the excess liquid, and cured at 80ºC for 10 min. The immersion-drying-curing cycle was applied one, two or three times, depending on the desired number of layers, Figure 1.

Ellipsometric measurements

The experimental set-up was similar to that used in previous works[21-24]. The sample was illuminated with monochromatic light in the wavelength visible range (400 nm < λ < 700 nm) with incident angles ϕ of 65º, 69º and 73º. Optical data were obtained by interposing filters corresponding to five λ (405, 450, 492, 546 or 580 nm). The sampled ellipsometric area, horizontally covered on the plaque, was about 0.5 mm^2 and the plaque geometric area 12 cm^2.

The ellipsometric parameters corresponding to the bare metal were obtained in a coating-free zone. The ellipsometric parameters Δ and ψ were recorded as a function of λ and the incident angle ϕ. Special care was taken to avoid modifying the alignment of the cell during each experiment.

CALCULATIONS

The simplest model assumes a single homogeneous film. The real part of the film refraction index, n, the imaginary part of the refraction index or absorption coefficient, k, and the thickness, d, are calculated using the gradient technique[25].

In the case of inhomogeneous layers, the high number of parameters makes the determination of the structure very cumbersome. However, the single homogeneous film model is a good first approximation in the interface description and these indices correspond to effective optical indices for the MPTMS/ porous layer composite[21-22, 24].

For a single Δ and ψ data the determination of n, k and d results are not univocal. In many simple processes the thickness layer grows with constant compactness and composition bearing stable n and k values. In this case assuming common n and k values the number of fitted parameters related to the number of data is strongly reduced. For example, two sets of Δ_1, ψ_1 and Δ_2, ψ_2, corresponding to d_1 and d_2 thicknesses respectively, allows the univocal determination of the four parameters n, k and d_1 and d_2. In many cases the fitting of the n, k and d values for a sequential set of thicknesses allows evaluating variations in the compactness of the film as a function of the distance to the electrode. In this procedure it is very important to use accurate initial values in the fitting, which can usually be found by fitting the complete set of thicknesses and, in a second step, by reducing the set of thicknesses and performing a new fitting with the optical constant obtained in the first step. Another possibility is to increase the amount of optical data for a given layer measuring the Δ and Ψ data at different λ_j. This allows increasing the amount of experimental data to find univocal values of thickness and optical constants.

The optical constants of the substrate were calculated assuming a simple air/metal interface free of optical surface layers. The Δ and ψ data corresponding to the metal surface in air, point 0, allows the determination of the n and k values of the substrate that remain constant after the coating deposition.

The fitting procedure minimizes the function G

$$G = \Sigma\ (\Delta^{ex}_{ijk} - \psi^{the}_{ijk})^2 + (\Delta^{ex}_{ijk} - \psi^{the}_{ijk})^2$$

where the sub index j corresponds to the optical data measured at different λ_j, different deposits or thickness d_i of the layer and in the case of the Procedure II, different incident angles ϕ.

The optimum theoretical Δ^{the}_{ijk}, ψ^{the}_{ijk} values are obtained minimizing the function G by means of a standard gradient method[25].

RESULTS AND DISCUSSION

Figure 2 shows the Δ and ψ data obtained applying one, two or three deposition steps using Procedure I. The figure also illustrates the calculated theoretical curves for several n and k values and the fitted curves obtained following the procedure described above. The MPTMS/ porous composite layer becomes attached through a thin iron oxide layer formed on the metal. The optical response $\delta\Delta = \Delta_{substrate} - \Delta_{substrate/oxide}$ of the layer is very low, $\delta\Delta$ < 0.5º and hence it can be neglected in the calculations[21-22]. The theoretical curves are plotted for thickness values between 10 nm and 240 nm, and with d increments every 10 nm. The theoretical curve

ORIGINAL ARTICLE

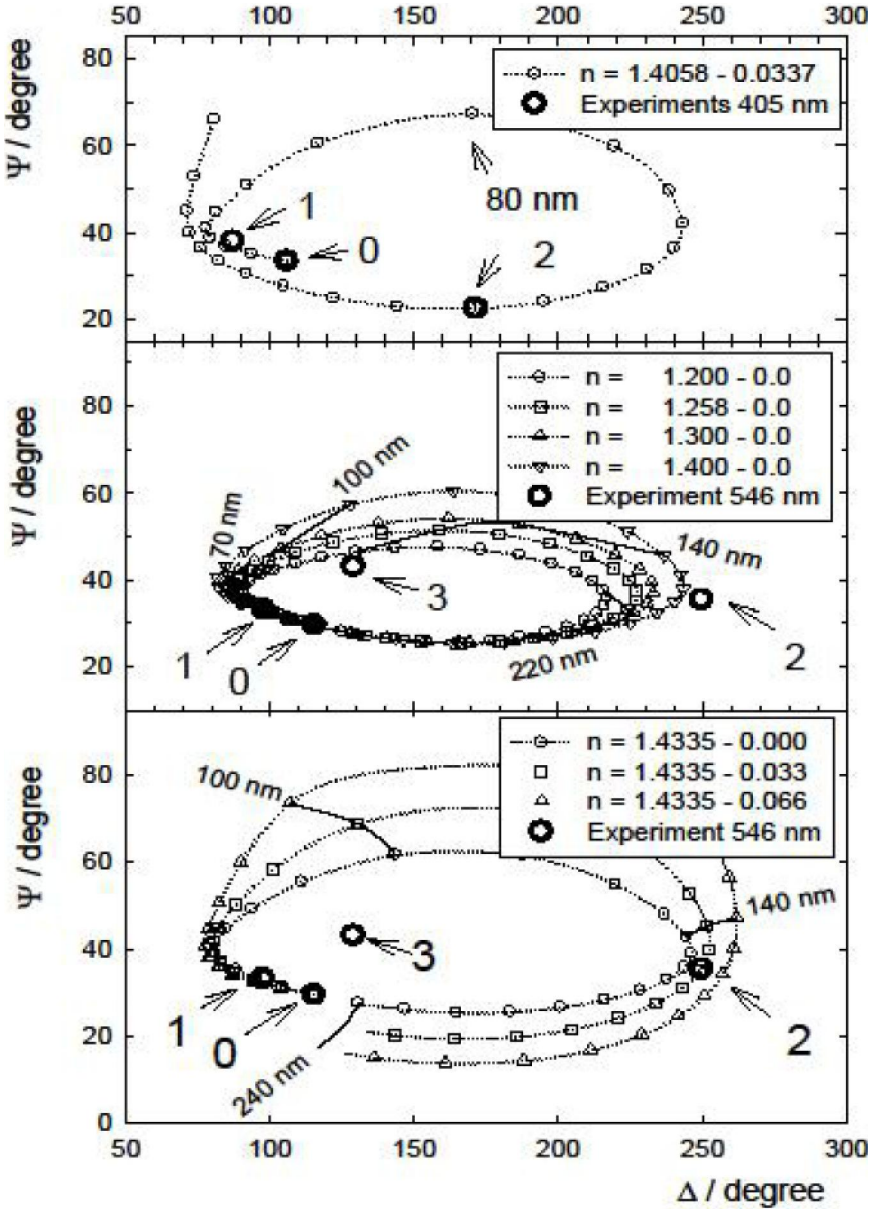

Figure 2 : Evolution of the ellipsometric parameters Δ and ψ for the sample prepared by successive deposition steps dipping in MPTMS 8 %, Procedure 1. (o) Experimental points: 0, for the substrate and 1, 2 and 3 after the deposition steps. (o, □, Δ, ∇ and point lines) Theoretical curves for increments of d= 10 nm assuming different effective optical constants n. The full line and the figures indicate the thickness d in nm. ϕ = 69°. a) λ = 405 nm, b) and c) λ = 546 nm.

(assuming optical indices independent of thickness) fits the experimental data in the whole range of thicknesses reproducing the several loops. After three deposition steps the films is so thick that only data at λ= 546 nm can be measured owing to the low intensity of the lamp and the maximal intensity at this λ, (Figure 2 b and c). The point 3 fits on the second semicircular loop and thickness values of about 350 nm.

Figure 2 b clearly shows that the fitted thickness of point 2 is very dependent on the n value, since thickness decreases with increasing n. The MPTMS coating is almost transparent with low k values and in several works the thickness is evaluated assuming k= 0[1, 6, 19]. However, the calculated d and n values are dependent on the k value and a more precise fitting can be obtained by fitting a large set of data obtained at several λ values and with k‘‘ 0. In these calculations a first approach is performed assuming common or average n and k values for the data set

ORIGINAL ARTICLE

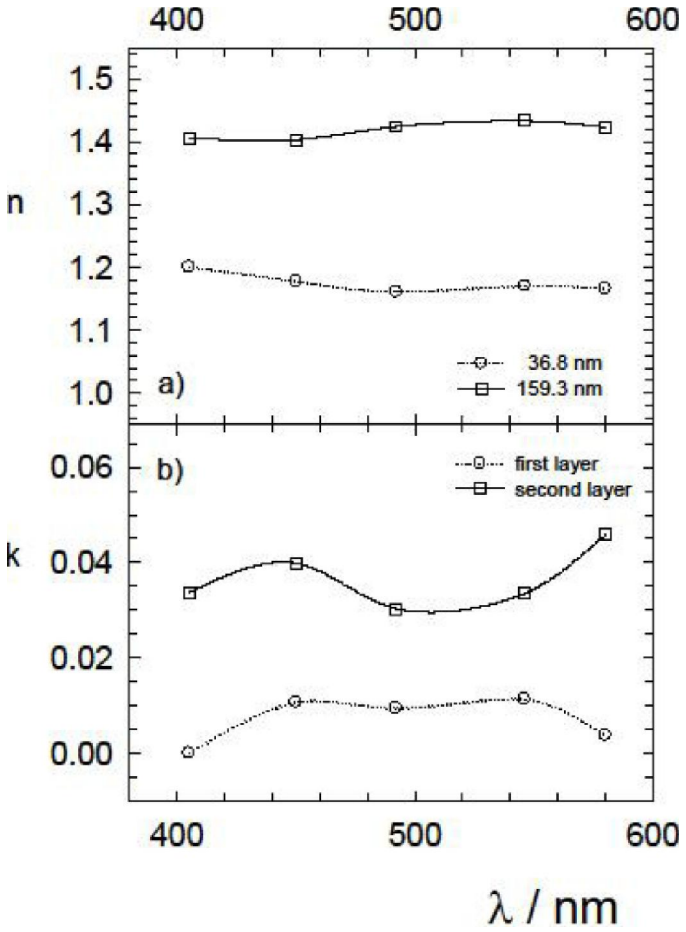

Figure 3 : Refraction index *n* vs. *λ* and absorption coefficients *k* vs. *λ* fitted for experiments corresponding to Procedure I. The figures indicate the fitted value of thicknesses obtained after 1 and 2 deposition steps.

corresponding to 1 and 2 deposition steps; in a second calculation the independent fitting of the point 1 and the point 2 is obtained with the data sets at five λ values starting with the initial condition obtained in the first approach.

Figure 3 shows the thicknesses *d* and refraction indices, *n*, *k*, vs. λ of the films calculated following the procedure mentioned above. The thickness of the layer increases four times with regard to the initial step, and it also becomes more compact. The very low value of G after the fitting shows that the isotropic and homogeneous single layer model is a good approach for the coatings description.

For isotropic materials, the *n* and *k* dependence on the composite volume fractions, *Q*, can be tested with effective medium theories, EMT[26-28]. Several models are proposed including the Maxwell-Garnett theory, the Bruggeman effective medium approximation, Lorentz-Lorenz, and the volume averaging theory, VAT, models. The *n* and *k* dependences on *d* and therefore the *n* vs *k* relationship allow setting the changes in *Q* or compactness of the film as a function of *d* through the adequate EMT[26-28]. For L/D ≥ 150, the film thickness *L* to pore diameter *D* ratio, the effective refraction index n_{eff} and the effective absorption index k_{eff} were determined to be independent of the pore diameter. In this case n_{eff} and k_{eff} depend only on porosity *Q* (pore phase volume to the total pore and MPTMS phase volume) and good agreement was found with predictions from the EMT[26-28]. In this case a quasi linear increase of n_{eff} and k_{eff} with *Q* is observed indicating an increase of more than 100% in *Q* with the second deposition step, Figure 3. Assuming a porosity $Q \approx 10$ % and an optical index $n = 1.6$ corresponding to the denser structure of MPTMS with high reticulation, for the first cover with $n = 1.2$, Procedure I, results 32 %, and for the second one with n= 1.42 a porosity of 65 %[6, 29, 30].

Figure 4 displays the Δ / ψ results after apply-

ORIGINAL ARTICLE

ing two deposition steps, Procedure II. The optical data correspond to measurements at three incident angles, namely 65°, 69° or 73° and five wavelengths. Figs. 3 a, and 3 b show data only for λ= 405 nm and λ= 546 nm. The decrease in the concentration of the silane solution produces a big change and a new picture in the Δ / ψ plot. The increase in the amount of data allows checking the validity of the single layer model for the coating characterization.

Figure 5 reproduces the data of Fig 4 b, showing the Δ and ψ data obtained at λ= 546 nm using Procedure II and applying one or two deposition steps. As seen, the calculated theoretical curves obtained for the fitted *n* and *k* values corresponding to both thicknesses are included. The theoretical curves are plotted for thicknesses between 10 nm < *d* < 240 nm, and *d* increases every 10 nm. The theoretical curves (assuming optical indices independent of the thickness) fit the experimental data obtained for the three angles ϕ.

In the initial part of the theoretical curves shown in Figure 5 for both layers, decreasing ψ values with quasi constant Δ were observed for small *d* values. By contrast, the theoretical curves of Figure 2 show decreasing Δ with small ψ increments. The change in ϕ yield a very great change in the Δ values for the first layer (Figugre 5 b). The theoretical fitting also shows a large dependence of Δ with respect to ϕ. However, the error in the fitting is higher than in the case of the second layer (Figure 5 a), probably due to higher inhomogeneity in the first cover and the dependence of the effective optical indices with respect to the pore size or anisotropy emergence. In this case the refraction n_{eff} and the effective absorption index k_{eff} calculated assuming an isotropic model should be considered as average optical indices, (Figure 6).

Figure 6 shows the optical indices dependence on λ for one or two deposition steps. The *n* indices are very low compared with those shown in Figure 3. This effect occurs together with relatively very high *k* indices.

Some of the EMT models have been derived by considering a unit cell containing one pore with uniform incident electromagnetic fields, thus ignoring possible interferences taking place between adjacent pores[26]. Large variations in n_{eff} and k_{eff} are observed for small *L*/*D* values using the VAT model

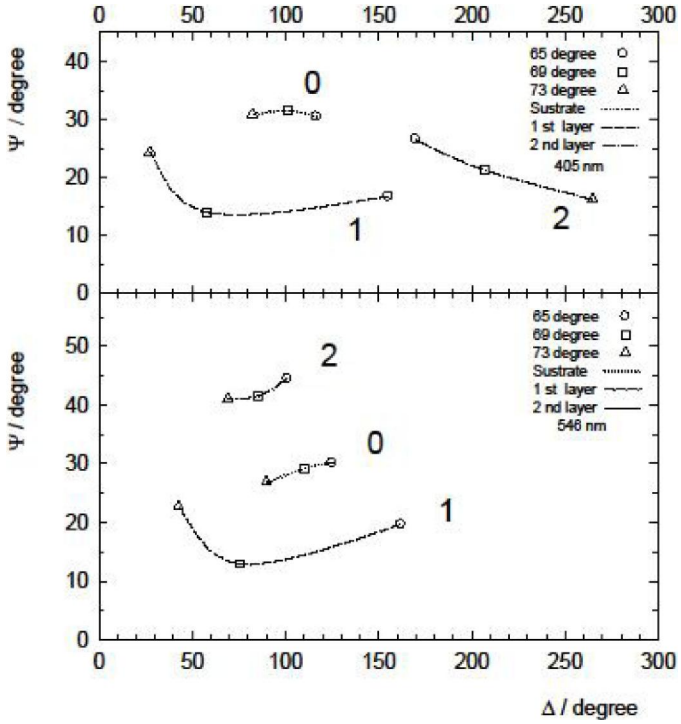

Figure 4 : Evolution of the ellipsometric parameters Δ and ψ for the sample prepared by successive deposition steps dipping in MPTMS 4 %, Procedure II. Experimental points: 0, for the substrate and 1, and 2 after the deposition steps. (o) ϕ= 65°, (□) ϕ= 69° and (Δ) ϕ= 73°. a) λ = 405 nm, b) λ = 546 nm.

ORIGINAL ARTICLE

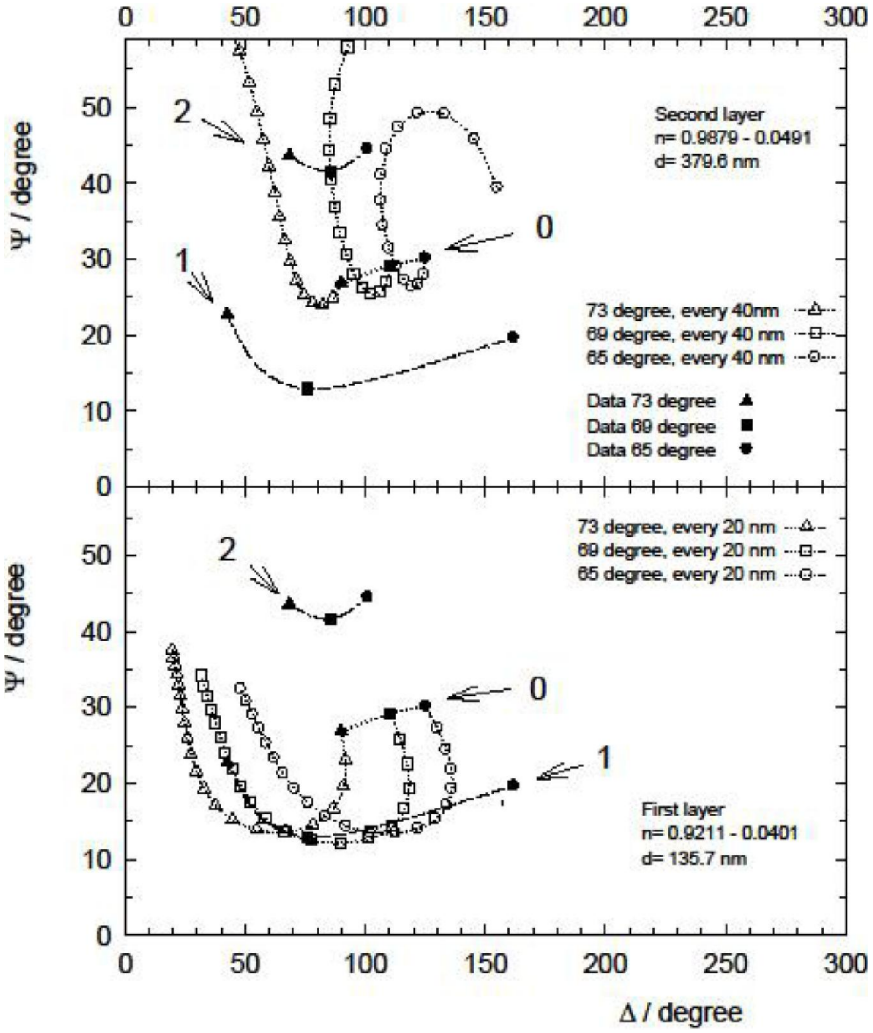

Figure 5 : As plotted in Figure 4 b. Experimental points using (●) ϕ= 65°, (■) ϕ= 69° and (▲) ϕ= 73°, λ = 546 nm. Point 0, indicates the substrate and points 1 and 2 after the data corresponding to the deposition steps. (Ë%, %, ²% and point lines). Theoretical curves for increments of *d*= 10 nm calculated with the fitted effective optical constants *n*, *k* for the data obtained at the different ϕ and λ .

and they are attributed to interferences between nanopores whose effect tends to average out if enough pores are considered. Beyond a critical film thickness to pore diameter ratio, $L/D > 150$ the pore shape has no effect on the effective optical properties. In these calculations the outer surface of the thin film is optically smooth and the possible film surface roughness is not accounted for, an aspect that can make the system more complex.

The VAT model also shows that under certain conditions, the effective refraction index of the composite material can be smaller and the absorption index higher than those of the continuous or dispersed phases. Similar results and conclusions are expected for different pores geometry[24, 26-28].

The effect of the curing conditions (baking temperature and time) on the optical transmittance has been reported[1, 6, 29-31]. The films obtained at low temperature and baked at 100 °C have high transmittance. These films contain a lot of hydroxyl or water molecules and the temperature rise during the heat treatment leads to a decrease in the hydroxyl content. The decrease in transmittance at 300 °C is attributed to a relatively large degree of light scattering from the pores[1].

The present results show that the decrease in the precursor concentration produces coats with higher porosity and optical absorption. Further work is needed to investigate the structure and composition of these films, their water content and the depen-

ORIGINAL ARTICLE

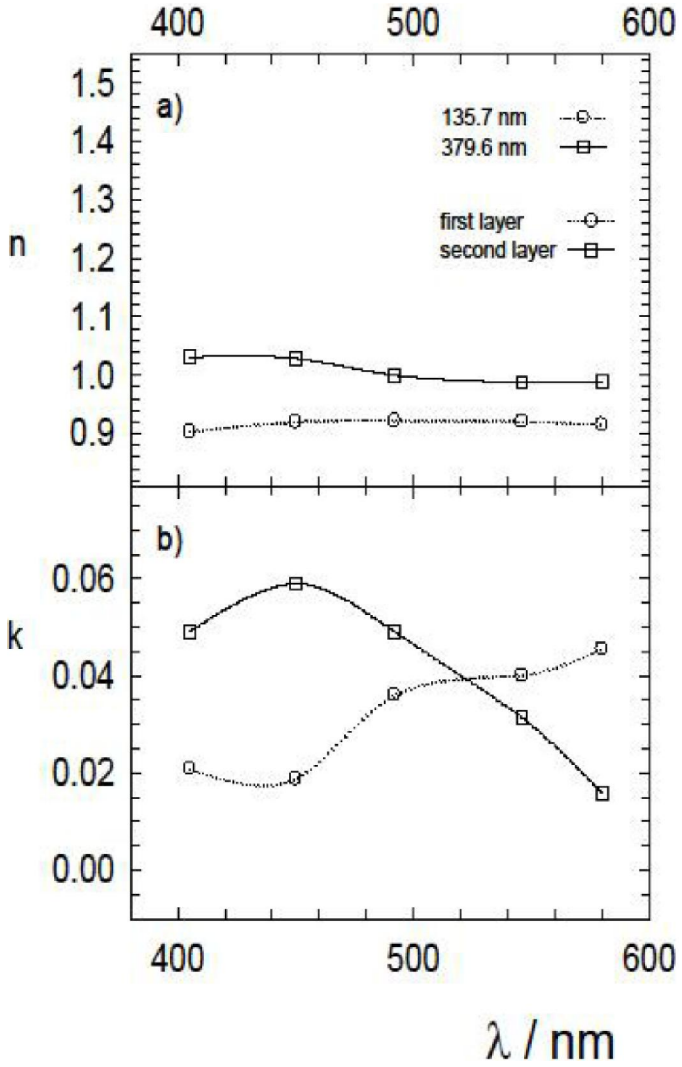

Figure 6 : Refraction index *n* vs. *λ* and absorption coefficients *k* vs. *λ* fitted for experiments corresponding to Procedure II. The figures indicate the fitted value of thicknesses obtained after 1 and 2 deposition steps

dence with respect to the precursor concentration. The higher optical indices and relatively lower absorption probably indicate that a higher solvent amount is retained within the most compact layers obtained using a higher precursor concentration.

CONCLUSIONS

The coats obtained with one or two deposition steps can be characterized with the homogeneous single model.

A significant increase in *d* and *Q* takes place after the second step. The initial coat works as template or substrate for the nucleation of the final layer.

For the higher promoter concentration the n_{eff} and k_{eff} increase after the second deposition step indicating an increase in *Q* ranging from 32% to 65 %.

The lower promoter concentration produces very low compact coats with low *Q* and relatively high *k* absorption values indicating that a strong interference occurs between adjacent pores. A concentration decrease probably leads to a decrease in the coat hydroxyl content.

ACKNOWLEDGEMENTS

This work was supported by the Consejo Nacional de Investigaciones Científicas (CONICET), the Comisión de Investigaciones Científicas de la Provincia de Buenos Aires (CIC). J. O. Z. is member of the Research Career of CIC. These results were presented at Nanocoatings 2013,

International Conference on Functional Nanocoatings. Politecnico of Milano, July 8-9 2013, www.nanocoatings2013.org.

REFERENCES

[1] W.Yuan, W.J.van Ooij; Characterization of organofunctional silane films on zinc substrates, J.Colloid Int.Sc., **185**, 197-209 **(1997)**.

[2] W.E.G.Hansal, S.Hansal, M.Pölzler, A.Kornherr, G.Zifferer, G.E.Nauer; Investigation of polysiloxane coatings as corrosion inhibitors of zinc surfaces, Surf.Coating Tech., **200**, 3056-3063 **(2006)**.

[3] W.J.van Ooij, D.Zhu, M.Stacy, A.Seth, T.Mugada, J.Gandhi, P.Puomi; corrosion protection properties of organofunctional silanes—an overview, Tsinghua Sci.Technol., **10**, 639-664 **(2005)**.

[4] W.J.van Ooij, D.Zhu; Corrosion protection of metals by water-based silane mixtures of bis-[trimethoxysilylpropyl]amine and vinyltriacetoxysilane.Prog.Org.Coat., **49**, 42-53 **(2004)**.

[5] W.J.van Ooij, T.F.Child; Protecting metals with silane coupling agents, Chemtech, **28**, 26-35 **(1998)**.

[6] A.Franquet, J.De Laet, T.Schram, H.Terryn, V.Subramanianb, W.J.van Ooij, J.Vereeckena; Determination of the thickness of thin silane films on aluminium surfaces by means of spectroscopic ellipsometry, Thin Solid Films, **384**, 37-45 **(2001)**.

[7] D.K.Aswal, S.Lenfant, D.Guerin, J.V.Yakhmi, D.Vuillaume; Tunnel current in self-assembled monolayers of 3-mercaptopropyltrimethoxysilane, Small, **1**, 725-729 **(2005)**.

[8] J.Wang, S.Yang, X.Liu, S.Ren, F.Guan, M.Chen; Preparation and characterization of ZrO_2 thin film on sulfonated self-assembled monolayer of 3-mercaptopropyl trimethoxysilane, Appl.Surf.Sci., **221**, 272-280 **(2004)**.

[9] J.Zhao, M.Chen, F.Yan; Preparation and micromechanical studies of polysiloxane containing dual layer film on Au surface, Colloids Surf.A.Physicochem.Eng.Aspect., **346**, 75-82 **(2009)**.

[10] M.L.Zheludkevich, R.Serra, M.F.Montemor, I.M.Miranda Salvado, M.G.S.Ferreira; Corrosion protective properties of nanostructured sol–gel hybrid coatings to AA2024-T3, Surf.Coat.Technol., **200**, 3084-3094 **(2006)**.

[11] M.A.Chen, X.Lu, Z.H.Guo, R.Huang; Influence of hydrolysis time on the structure and corrosion protective performance of (3-mercaptopropyl)triethoxysilane film on copper, Corr.Sci., **53**, 2793-2802 **(2011)**.

[12] U.Bexell, T.M.Grehk; A corrosion study of hot-dip galvanized steel sheet pre-treated with γ-mercaptopropyltrimethoxysilane, Surf.Coat.Technol., **201**, 4734-4742 **(2007)**.

[13] D.Zhu, W.J.van Ooij; Structural characterization of bis-[triethoxysilylpropyl] tetrasulfide and bis-[trimethoxysilylpropyl]amine silanes by Fourier-transform infrared spectroscopy and electrochemical impedance spectroscopy, J.Adhesion Sci.Technol., **16**, 1235-1260 **(2002)**.

[14] D.Zhu, W.J.van Ooij; Corrosion protection of AA 2024-T3 by bis-[3-(triethoxysilyl) propyl] tetrasulfide in sodium chloride solution.: Part 2: mechanism for corrosion protection, J.Corros.Sci., **45**, 2177-2197 **(2003)**.

[15] D.Zhu, W.J.van Ooij; Enhanced corrosion resistance of AA 2024-T3 and hot-dip galvanized steel using a mixture of bis-[triethoxysilylpropyl]tetrasulfide and bis-[trimethoxysilylpropyl]amine, Electrochim.Acta, **49**, 1113-1125 **(2004)**.

[16] P.R.Seré, C.Deyá, W.A.Egli, C.I.Elsner, A.R.Di Sarli; Protection of galvanized steel with silanes: Its Comparison with Chromium(VI), J.of Mater.Eng.Perform., **23**, 342-348 **(2014)**.

[17] W.Que, Z Sun, Y.Zhou, Y.Lam, Y.Chan, C.Kam; Optical and mechanical properties of TiO_2/SiO_2/organically modified silane composite films prepared by sol–gel processing, Thin Solid Films, **359**, 177-183 **(2000)**.

[18] P.Macech, J.E.Pemberton; Ultrathin silica films immobilized on gold supports: Fabrication, Characterization, and Modification, *Langmuir, **23,*** 9816-9822 ***(*2007)**.

[19] W.R.Thompson, M.Cai, M.Ho, J.E.Pemberton; Hydrolysis and condensation of self-assembled monolayers of (3-mercaptopropyl) trimethoxysilane on ag and au surfaces, *Langmuir, **13,*** 2291-2302 **(1997)**.

[20] E.Besson, A.M.Gue, J.Sudor, H.K.Youssoufi, N.Jaffrezic, J.Tardy; A novel and simplified procedure for patterning hydrophobic and hydrophilic SAMs for microfluidic devices by using UV photolithography, *Langmuir,* **22**, 8346-8352 **(2006)**.

[21] J.O.Zerbino, O.L.Bulhoes, S.Juanto, M.I.Miguez, J.R.Vilche, A.J.Arvia; Ellipsometry of iron hydrous oxide layers formed by potentiodynamic techniques, Thin Solid Films, **233**, 74-76 **(1993)**.

ORIGINAL ARTICLE

[22] O.A.Albani, J.O.Zerbino, J.R.Vilche, A.J.Arvia; A comparative electrochemical and ellipsometric study of iron electrodes in different alkaline electrolytes, Electrochim.Acta, **31**, 1403-1411 **(1986)**.

[23] J.O.Zerbino, A.Maltz, C.Falivene, N.E.Avaca, M.G.Sustersic, S.Siboni, C.Della Volpe; Electrochemical and optical study of the confined aqueous layer adsorbed on Gold Electrodes cycled in phosphate and dodecylsulphate solutions, J.Appl.Electrochem, **44**, 1355-1360 **(2014)**.

[24] V.Toranzos, J.O.Zerbino, A.Maltz, G.Ortiz; Ellipsometric study of semitransparent Silver Layers deposited on glass.Av.Cien.Ing., **5**, 67-65 **(2014)**.

[25] G.Dahlquist, A.Björck; Numerical methods, Prentice-Hall, Englewood Cliffs, New Jersey, Editions, Cap.10, Sección 5.2, **(1974)**.

[26] A.Garahan, L.Pilon, J.Yin, I.Saxena; Effective optical properties of absorbing nanoporous and nanocomposite thin films, J.Appl.Physics, **101**, 014320-1-9 **(2007)**.

[27] N.J.Hutchinson, A.Navid, T.Coquil, L.Pilon; Effective optical properties of highly ordered mesoporous thin films, Thin Solid Films, **518**, 2141-2146 **(2010)**.

[28] N.J.Hutchinson, T.Coquil, E.Richman, S.Tolbert, L.Pilon; reflectance of surfactant-templated mesoporous silica thin films: *simulations versus experiments,* Thin Solid Films, **518**, 2134-2140 **(2010)**.

[29] G.Ouyang, K.Wang, L.Henriksen, M.N.Akram, X.Y.Chen; A novel tunable grating fabricated with viscoelastic polymer (PDMS) and conductive polymer (PEDOT), Sensors Actuators A, **158**, 313-319 **(2010)**.

[30] A.Franquet, H.Terryn, P.Bertrand, J.Vereecken; Use of optical methods to characterize thin silane films coated on aluminium, Surf.Interf.Anal., **34**, 25-29 **(2002)**.

[31] I.De Graeve, J.Vereecken, A.Franquet, T.Van Schaftinghen, H.Terryn; Silane coating of metal substrates: Complementary use of electrochemical, Optical and thermal analysis for the evaluation of film properties, Prog.Org.Coat., **59**, 224-229 **(2007)**.